J Nanostruct 16(1): 916-931, Winter 2026

RESEARCH PAPER

Application of Hydroxyapatite Nanoparticles Incorporated on $AgFe_2O_4$ Magnetic Nanoparticles in Dental Implant

Azimov Aziz [1] *, Nilufar Sharipova [2], Mamatkulova Mokhigul [3], Islomova Odina [4], Sait A. Abkerimov [5], Abitov Ilnur [6], Aslonova Ibodat [7], Narziyev Shamsidin [8], Rayhon Hotamova [7], Khazratov Utkir [7], Bakhronov Sherzod [9], Qushnazarova Ugiljon [10], Abdurashidov Akhror [11]

[1] *Department of Surgical Dentistry and Dental Implantology, Tashkent State Medical University, Tashkent, Republic of Uzbekistan*

[2] *Department of Russian Language and Literature, Bukhara State Pedagogical Institute, Bukhara, Republic of Uzbekistan*

[3] *Department of Obstetrics and Gynecology No.2, Samarkand State Medical University, Samarkand, Republic of Uzbekistan*

[4] *Department of Pedagogy and Teaching languages, Urgut Branch of Samarkand State University named after Sharof Rashidov, Samarkand, Republic of Uzbekistan*

[5] *Tashkent State Technical University, Tashkent, Republic of Uzbekistan*

[6] *Department of Agronomy, Navoi State Mining and Technological University, Navoi, Republic of Uzbekistan*

[7] *Department of Propaedeutics of Internal Medicine, Bukhara State Medical Institute, Bukhara, Republic of Uzbekistan*

[8] *Department of Propaedeutics of Internal Diseases, Bukhara State Medical Institute, Bukhara, Republic of Uzbekistan*

[9] *Department of Medical Fundamental Sciences, Kimyo International University in Tashkent, Samarkand Branch, Samarkand, Uzbekistan*

[10] *Urgench state university, Urgench, Uzbekistan*

[11] *Department of Urology and Oncology, Fergana Medical Onstitute of Public Health, Fergana, Republic of Uzbekistan*

ARTICLE INFO

Article History:
Received 02 September 2025
Accepted 18 December 2025
Published 01 January 2026

Keywords:
$AgFe_2O_4$
Dental implant
Hydroxyapatite
Magnetic nanoparticle
Nanoparticles

ABSTRACT

This study presents the design and comprehensive evaluation of a novel "smart" nanocomposite coating. A core-shell architecture was engineered by integrating silver ferrite ($AgFe_2O_4$) magnetic nanoparticles with a bioactive hydroxyapatite (HAp) shell. The $AgFe_2O_4$ core provides both sustained antimicrobial silver ion release and magnetic responsiveness, while the HAp shell ensures osteoconductivity. A sequential solvothermal and wet-chemical precipitation synthesis yielded a well-defined HAp@ $AgFe_2O_4$ nanocomposite, as confirmed by XRD, TEM, and FT-IR analysis. This material was processed into a uniform, adherent coating on Ti-6Al-4V substrates. *In vitro* studies demonstrated the coating›s high bioactivity, with a significant apatite-forming ability in simulated body fluid (mass gain of 1.52 mg/cm² after 21 days). The coating exhibited potent passive antibacterial efficacy (>88% reduction) against *S. mutans* and *P. gingivalis*. Crucially, exposure to an alternating magnetic field (350 kHz, 12 kA/m) triggered on-demand hyperthermia (ΔT = 12.5 °C), enhancing bacterial eradication to >97%. Furthermore, the coating supported human osteoblast (MG-63) proliferation and significantly increased alkaline phosphatase activity (1.6-fold vs. control), indicating enhanced osteogenic differentiation. The results confirm the successful creation of a dual-functional, magnetically responsive coating that synergistically promotes bone integration while offering a powerful, triggerable defense against infection, representing a significant advance towards intelligent dental implant surfaces.

How to cite this article
Aziz A., Sharipova N., Mokhigul M. et al. Application of Hydroxyapatite Nanoparticles Incorporated on $AgFe_2O_4$ Magnetic Nanoparticles in Dental Implant. J Nanostruct, 2026; 16(1):916-931. DOI: 10.22052/JNS.2026.01.081

* *Corresponding Author Email: ziza97.aa@gmail.com*

INTRODUCTION

The integration of nanotechnology into dental implantology represents a paradigm shift from a purely mechanical approach to a bioactive, strategically engineered one [1-5]. Historically, the quest for osseointegration the direct structural and functional connection between living bone and the implant surface has driven material innovation from macro-scale modifications to micro-rough topographies [6-8]. The advent of nanotechnology has further refined this trajectory, enabling precise manipulation at the molecular and cellular level to directly modulate biological responses. Nanostructured coatings, notably those based on calcium phosphate ceramics like hydroxyapatite (HAp), have been extensively explored to mimic the native bone matrix, thereby enhancing osteoblast adhesion, proliferation, and differentiation [9]. However, critical challenges persist, including the inherent brittleness and poor adhesion of pure HAp coatings to metallic substrates, as well as the lack of inherent functionality to combat peri-implantitis, a leading cause of implant failure [10-12]. Furthermore, achieving controlled, localized delivery of therapeutic agents or ions at the implant-tissue interface remains a significant hurdle. Consequently, contemporary research focuses on developing advanced nanocomposite systems that synergize the bioactivity of HAp with functional properties such as antimicrobial activity,

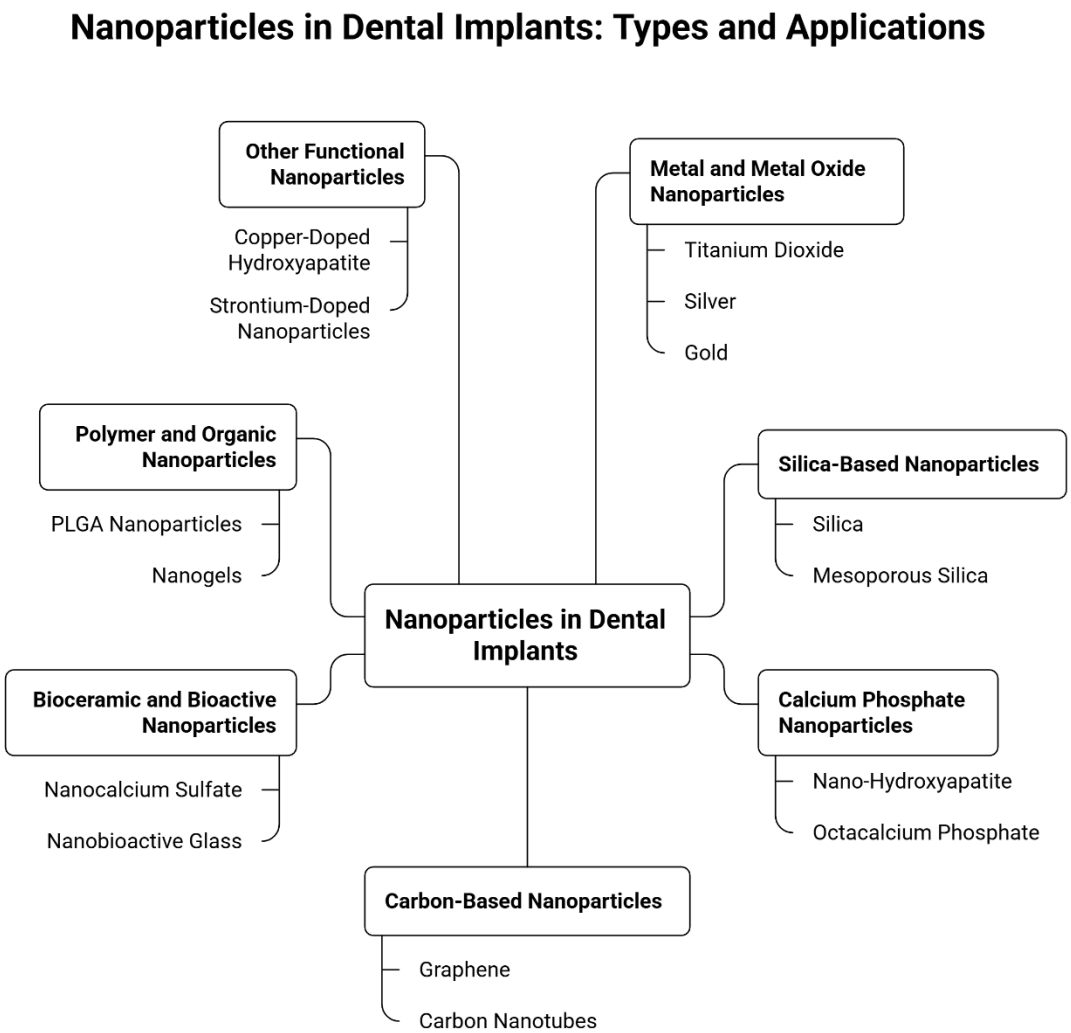

Fig. 1. Different nanoparticles applied in dental implants

improved mechanical resilience, and stimuli-responsiveness to address these multifaceted demands and propel the next generation of "smart" dental implants [13-16]. Fig. 1 displays different nanoparticles applied in dental implants.

Recent advancements in dental implantology have increasingly leveraged the unique physicochemical properties of nanoparticles to engineer surfaces that actively promote osseointegration and confer antimicrobial resistance. Moving beyond passive micron-scale roughening, contemporary strategies employ nanoparticles of bioactive glasses, titanium dioxide, zinc oxide, and, predominantly, hydroxyapatite (HAp) to create nanotextured topographies. These nanostructures significantly enhance the surface energy and effective surface area, which in turn improves protein adsorption and provides more favorable sites for osteogenic cell attachment and proliferation [16]. A key advantage of nanoparticle coatings is their ability to act as reservoirs for the controlled release of therapeutic ions (e.g., Ag^+, Zn^{2+}, Sr^{2+}) or drugs [17, 18], offering a potent strategy to mitigate biofilm formation and prevent peri-implantitis. Furthermore, nanocomposite systems, where HAp is combined with polymers or other inorganic phases, have been developed to address the poor mechanical cohesion and brittleness of pure HAp films [19]. Despite these promising developments, significant disadvantages and unresolved problems remain. The long-term stability of the nanoparticle-substrate interface under cyclic masticatory loading is often insufficient, leading to delamination [20]. The antimicrobial efficacy of many doped systems is either non-persistent, prone to inducing bacterial resistance (in the case of certain antibiotic loadings), or cytotoxic at concentrations required for effectiveness. Moreover, a critical gap exists in achieving spatiotemporally controlled therapeutic action once implanted, the functionality is static [21]. There is a pressing need for "smart" implants whose surface activity, such as targeted antimicrobial ion release, can be triggered on-demand in response to a pathological stimulus, thereby maximizing therapeutic efficacy while minimizing off-target effects and preserving the surrounding healthy tissue. This represents a formidable materials chemistry challenge, requiring the integration of multifunctional, responsive nanocarriers into a robust, osteoconductive matrix [22].

this study aims to design, synthesize, and comprehensively characterize a novel multifunctional nanocomposite coating for dental implants. The core innovation lies in the strategic incorporation of silver-doped iron oxide ($AgFe_2O_4$) magnetic nanoparticles as a functional platform, onto which a bioactive layer of hydroxyapatite (HAp) nanoparticles is integrated. We hypothesize that this architecture will synergistically couple the established osteoconductivity of HAp with the dual capability of the $AgFe_2O_4$ phase: firstly, to provide sustained antimicrobial activity through the controlled release of Ag^+ ions, and secondly, to introduce magnetic responsiveness. It is this latter property that we specifically target to address the critical problem of non-selective, static antibacterial action in current systems.

MATERIALS AND METHODS

Materials and Apparatus

All chemical reagents were of analytical grade and utilized as received without further purification. Calcium nitrate tetrahydrate ($Ca(NO_3)_2{\cdot}4H_2O$, ≥99.0%), diammonium hydrogen phosphate ($(NH_4)_2HPO_4$, ≥99.0%), and ammonium hydroxide solution (NH_4OH, 28–30% NH_3 basis) were procured from Sigma-Aldrich (Germany) for the synthesis of hydroxyapatite. The precursors for the magnetic carrier, silver nitrate ($AgNO_3$, ≥99.8%) and iron(III) nitrate nonahydrate ($Fe(NO_3)_3{\cdot}9H_2O$, ≥98%), were obtained from Merck (Germany). Ethylene glycol (EG, 99%) and sodium hydroxide (NaOH, pellets, 97%) were supplied by Alfa Aesar (UK). Absolute ethanol (C_2H_5OH, 99.9%) was used for washing procedures. Medical-grade titanium alloy (Ti-6Al-4V) discs (10 mm diameter, 2 mm thickness) were purchased from Baoji Xinlian Titanium Industry Co., Ltd. (China) and sequentially polished with silicon carbide paper (up to 2000 grit) and washed ultrasonically in acetone, ethanol, and deionized water prior to coating. The synthesis of $AgFe_2O_4$ magnetic nanoparticles (MNPs) and their subsequent functionalization with hydroxyapatite (HAp) nanoparticles were performed using a programmable hotplate stirrer (IKA® RCT digital) equipped with precise temperature control. A high-intensity ultrasonic probe (Sonics & Materials Vibra-Cell VCX 750, 750 W, 20 kHz) was employed for the dispersion of nanoparticles in suspension and during the coating process. A comprehensive suite of characterization techniques was utilized to analyze the structure,

morphology, and composition of the synthesized nanocomposites. Powder X-ray diffraction (XRD) patterns were recorded on a Rigaku SmartLab X-ray diffractometer (Japan) operating with Cu Kα radiation (λ = 1.5406 Å) at 40 kV and 40 mA. Data were collected in the 2θ range of 10° to 80° with a step size of 0.02°. Fourier-transform infrared (FT-IR) spectroscopy was performed on a Bruker ALPHA II Platinum ATR spectrometer (Germany) in the range of 400–4000 cm^{-1} with a spectral resolution of 4 cm^{-1}. The morphological features and elemental composition of the samples were investigated using a field-emission scanning electron microscope (FE-SEM, Tescan GAIA3, Czech Republic) equipped with an Oxford Instruments X-MaxN 80 ev, operating at an accelerating voltage of 15 kV. For transmission electron microscopy (TEM) analysis, a drop of the nanoparticle suspension in ethanol was deposited onto a carbon-coated copper grid. Images and selected-area electron diffraction (SAED) patterns were acquired using a JEOL JEM-2100F field-emission transmission electron microscope (Japan) operated at 200 kV. The magnetic properties of the $AgFe_2O_4$ MNPs were evaluated using a vibrating sample magnetometer (VSM, Lake Shore 7404, USA) at room temperature, applying a magnetic field of up to ±20 kOe.

Preparation of Hydroxyapatite Nanoparticles Incorporated on $AgFe_2O_4$ Magnetic Nanoparticles

The core-shell nanocomposite, designated as HAp@$AgFe_2O_4$, was synthesized via a sequential, two-step wet-chemical route designed to ensure a uniform coating of bioactive hydroxyapatite onto the magnetic core.

Step 1: Synthesis of $AgFe_2O_4$ Magnetic Nanoparticles (MNPs)

Silver-iron oxide nanoparticles were prepared through a modified solvothermal co-precipitation method. Briefly, equimolar aqueous solutions of $Fe(NO_3)_3 \cdot 9H_2O$ (0.2 M) and $AgNO_3$ (0.1 M) were combined in a 2:1 molar ratio (Fe:Ag) under vigorous magnetic stirring. To this mixture, 150 mL of ethylene glycol, acting as both solvent and reducing agent, was added dropwise. The pH of the resulting solution was subsequently adjusted to 11.0 by the controlled addition of 5 M NaOH solution, which initiated the immediate formation of a dark brown precipitate. The suspension was then transferred into a 250 mL Teflon-lined stainless-steel autoclave, sealed, and maintained at 180 °C for 18 hours in a laboratory oven. After cooling naturally to ambient temperature, the obtained black precipitate was collected using a neodymium magnet, washed sequentially with deionized water and absolute ethanol until the supernatant reached neutrality (pH ~7), and finally dried under vacuum at 60 °C for 12 hours. The product was lightly ground in an agate mortar to obtain a fine $AgFe_2O_4$ nanopowder [23].

Step 2: In-situ Precipitation of Hydroxyapatite onto $AgFe_2O_4$ MNPs

The deposition of a hydroxyapatite (HAp) shell was achieved via an in-situ chemical precipitation method in an aqueous medium maintained at physiological pH. First, 500 mg of the as-synthesized $AgFe_2O_4$ MNPs were uniformly dispersed in 200 mL of deionized water using a 750 W ultrasonic probe for 30 minutes to break any soft agglomerates. This stable magnetic colloid was then transferred to a three-neck round-bottom flask equipped with a mechanical overhead stirrer (500 rpm) and a water bath for precise temperature control. Separately, precursor solutions of 0.5 M $Ca(NO_3)_2 \cdot 4H_2O$ and 0.3 M $(NH_4)_2HPO_4$ were prepared, maintaining a Ca/P molar ratio of 1.67. Under constant stirring, the calcium solution was introduced into the $AgFe_2O_4$ suspension. The phosphate solution was then added dropwise at a controlled rate of 2 mL min^{-1} using a peristaltic pump. Concurrently, the pH of the reaction mixture was meticulously held at 9.5 ± 0.2 by the automated addition of dilute NH_4OH, a condition known to favor the formation of stoichiometric HAp. The reaction was allowed to proceed at 80 °C for 4 hours under a N_2 atmosphere to minimize carbonate incorporation. The resulting composite particles were magnetically separated, washed thoroughly with warm deionized water and ethanol, and subjected to freeze-drying (Christ Alpha 1-4 LDplus) for 48 hours to obtain a fluffy, agglomerate-free powder of the final HAp@$AgFe_2O_4$ nanocomposite [24].

Coating Deposition and In Vitro Biofunctional Evaluation

The biofunctional efficacy of the HAp@$AgFe_2O_4$ nanocomposite was evaluated through a series of *in vitro* assays designed to simulate the dental implant environment. Medical-grade Ti-6Al-4V alloy discs were used as substrates. Prior to coating, the discs underwent a three-step ultrasonic cleaning

protocol in acetone, ethanol, and deionized water for 15 minutes each, followed by drying under a nitrogen stream. A stable, homogeneous coating suspension was prepared by dispersing 50 mg of the HAp@$AgFe_2O_4$ nanocomposite powder in 10 mL of a 2% (v/v) polyvinylpyrrolidone (PVP, MW ~40,000) ethanolic solution under ultrasonication for 60 minutes. The coatings were then applied onto the pre-treated Ti discs via a spin-coating technique (Laurell WS-650MZ-23NPPB) at 3000 rpm for 30 seconds, repeated for three layers with intermediate drying at 80°C for 5 minutes. Finally, the coated discs were subjected to a mild thermal treatment at 300°C for 2 hours in a tube furnace under an argon atmosphere to enhance coating adhesion and crystallinity without compromising the magnetic properties of the core [25].

Biofunctional Characterization Protocols
Coating Adhesion and Stability

The adhesive strength of the composite coating to the Ti substrate was assessed using a micro-scratch tester (Anton Paar Revetest) equipped with a Rockwell C diamond stylus (200 µm radius). Scratches were performed under a linearly increasing load from 10 mN to 5 N over a 5 mm track length at a speed of 5 mm/min. The critical load (Lc) for coating failure was determined via *in-situ* acoustic emission and optical microscopy. Furthermore, coating stability was evaluated by immersing the coated discs in 20 mL of simulated body fluid (SBF, prepared according to Kokubo's protocol) at 37°C under gentle agitation (100 rpm) for 28 days. The mass loss of the coating and the ionic concentration of Ca^{2+}, Ag^{+}, and Fe^{3+} in the SBF were monitored weekly using inductively coupled plasma optical emission spectrometry (ICP-OES, PerkinElmer Avio 500) [26].

In Vitro Bioactivity (Apatite-Forming Ability)

The bioactivity of the coated surfaces was evaluated by monitoring the formation of a bone-like apatite layer after immersion in SBF. The HAp@$AgFe_2O_4$-coated and uncoated control Ti discs were immersed in 30 mL of SBF at 37°C for periods of 7, 14, and 21 days. After each interval, the discs were removed, rinsed gently with deionized water, and dried [27].

Antibacterial Efficacy (Static and Magnetic-Field Triggered)

The antibacterial performance was quantified against two representative oral pathogens: *Streptococcus mutans* (ATCC 25175, Gram-positive) and *Porphyromonas gingivalis* (ATCC 33277, Gram-negative), using a modified ISO 22196:2011 protocol.

Static Release Assay: Bacterial suspensions (100 µL, ~1 x 10^6 CFU/mL in nutrient broth) were inoculated onto the surface of coated and control discs and incubated for 24 hours at 37°C under anaerobic conditions (80% N_2, 10% H_2, 10% CO_2). The viable bacteria were then eluted, serially diluted, and plated to determine the colony-forming units (CFU) [28].

Magneto-Thermal Triggered Assay: To evaluate the on-demand therapeutic potential, discs with adhered bacteria (after 12 hours of pre-incubation) were exposed to an alternating magnetic field (AMF) using a custom-built induction heating system (Ambrell EASYHEAT 2.4 kW, coil diameter 3 cm). The field parameters were set to a frequency of 350 kHz and a field strength of 12 kA/m, applied in four cycles of 5 minutes ON / 10 minutes OFF. The local temperature increase at the disc surface was monitored in real-time using a fiber-optic thermometer (Opsens, ZT-PT-N1400). Bacterial viability was assessed immediately after the AMF treatment cycle. The antibacterial rate (R, %) was calculated as R = [(A - B) / A] x 100, where A and B are the CFU counts from the control and test samples, respectively [29].

Cytocompatibility and Osteogenic Activity

The cytocompatibility of the coatings was evaluated using human osteoblast-like cells (MG-63, ATCC CRL-1427). Cells were seeded on the coated discs at a density of 1 x 10^4 cells/cm^2 and cultured in Dulbecco's Modified Eagle Medium (DMEM) supplemented with 10% fetal bovine serum. Cell viability and proliferation were assessed after 1, 3, and 7 days using the AlamarBlue assay (n=6). The osteogenic differentiation potential was evaluated by measuring the alkaline phosphatase (ALP) activity of the cells after 7 and 14 days of culture in osteogenic medium, normalized to the total protein content [30].

RESULTS AND DISCUSSION

Synthesis of HAp@$AgFe_2O_4$ Nanocomposite

The HAp@$AgFe_2O_4$ core-shell nanocomposite was successfully synthesized through a sequential two-step strategy, as delineated in the experimental section, with each step meticulously

designed to achieve specific structural and functional objectives.

The initial synthesis of the magnetic core, $AgFe_2O_4$ nanoparticles, employed a solvothermal co-precipitation method using ethylene glycol as a solvent. This approach was selected for its ability to produce nanoparticles with high crystallinity and controlled morphology, which are critical for maintaining strong magnetic properties. The elevated temperature (180 °C) and extended reaction time (18 h) within the autoclave facilitate the Ostwald ripening process, yielding particles with uniform size and well-defined spinel structure, essential for consistent magnetic response. The 2:1 Fe:Ag precursor ratio directly targets the stoichiometry of the $AgFe_2O_4$ phase, while ethylene glycol concurrently acts as a reducing agent, ensuring the incorporation of Ag^+ into the ferrite lattice rather than its segregation as metallic silver [31].

Subsequently, the bioactive hydroxyapatite (HAp) shell was deposited onto the pre-formed magnetic cores via an *in-situ* wet-chemical precipitation. This step is crucial for creating a direct interface between the two phases, promoting strong interfacial bonding critical for coating integrity under mechanical stress [32]. The $AgFe_2O_4$ nanoparticles were first exfoliated via ultrasonication to prevent magnetic aggregation and ensure a homogeneous dispersion, a prerequisite for a uniform coating. The precipitation was conducted under strict kinetic control: the dropwise addition of the phosphate precursor at a rate of 2 mL min^{-1}, coupled with rigorous stirring, prevents the homogeneous nucleation of pure HAp in the bulk solution, instead favoring heterogeneous nucleation on the magnetic nanoparticle surfaces. Maintaining the reaction pH at 9.5 ± 0.2 is deliberate, as this alkaline environment is optimal for the formation of stoichiometric, crystalline HAp while suppressing the formation of other calcium phosphate phases like brushite or monetite. The mild reaction temperature of 80 °C accelerates crystallization without compromising the pre-existing $AgFe_2O_4$ core, and the inert N_2 atmosphere minimizes carbonate substitution in the HAp lattice, preserving its bioactivity and dissolution profile. The final freeze-drying step was implemented to obtain a dry, aerated powder, effectively mitigating hard agglomeration caused by capillary forces during conventional oven drying, thereby

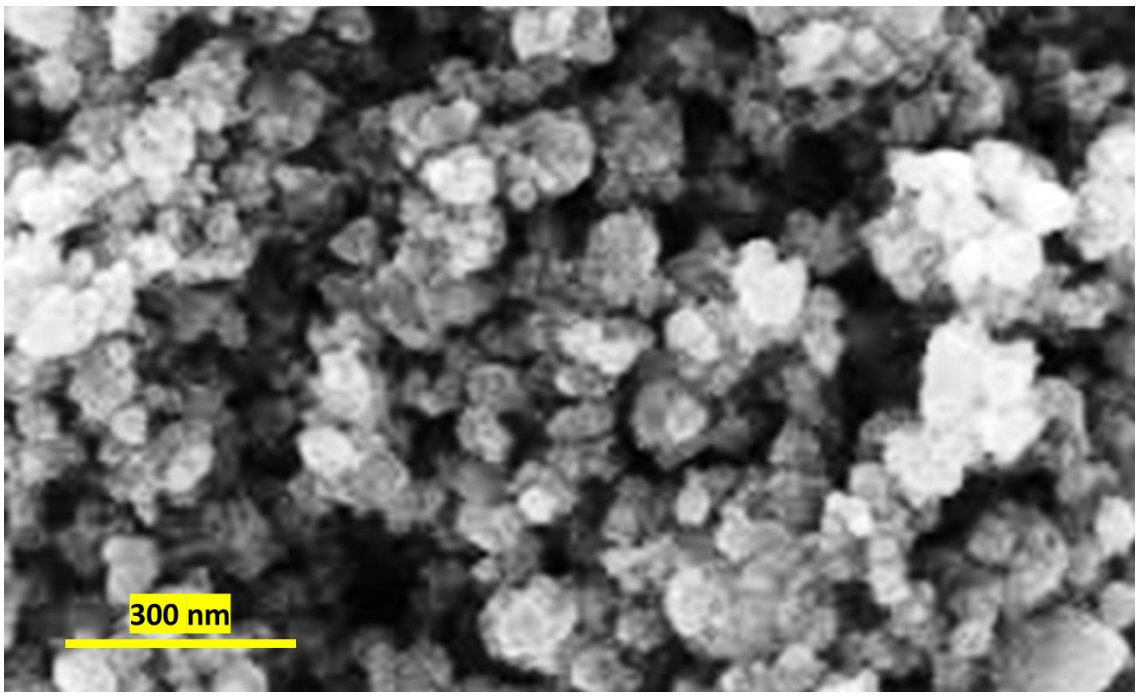

Fig. 2. FE-SEM images of HAp@$AgFe_2O_4$ nanocomposite

preserving the nanoscale features and ensuring the material's suitability for subsequent coating applications [33].

Characterization of HAp@$AgFe_2O_4$ Nanocomposite

The surface morphology of the final HAp@$AgFe_2O_4$ nanocomposite was investigated using FE-SEM. The representative micrograph presented in Fig. 2 reveals a successful and distinct architectural transformation from the precursor magnetic nanoparticles. The image confirms the formation of discrete, yet partially aggregated, nanocomposite structures. The primary particles exhibit a core-shell morphology, where the underlying $AgFe_2O_4$ cores, synthesized in the initial step, are visibly coated with a layer of finer, acicular crystallites. These needle-like features, with dimensions ranging from approximately 20-30 nm in width and 50-150 nm in length, are characteristic of crystalline hydroxyapatite. The uniformity of this coating across the micrograph suggests that the *in-situ* precipitation strategy, particularly the pre-dispersion of the magnetic cores via ultrasonication and the controlled dropwise addition of precursors, was effective in promoting heterogeneous nucleation on the nanoparticle surfaces. This process successfully mitigated the homogeneous nucleation of pure HAp in the bulk solution, a common pitfall of such co-precipitation methods. The resulting microstructure is notably porous and textured, creating a high-surface-area topography. This nanoscale roughness is a critical morphological attribute for a dental implant coating, as it is directly correlated with enhanced protein adsorption, improved wettability, and superior mechanical interlocking with growing bone tissue, thereby potentially accelerating the osseointegration process.

The intimate core-shell architecture of the HAp@$AgFe_2O_4$ nanocomposite was unequivocally resolved using TEM. The representative micrograph in Fig. 3 provides definitive nanoscale

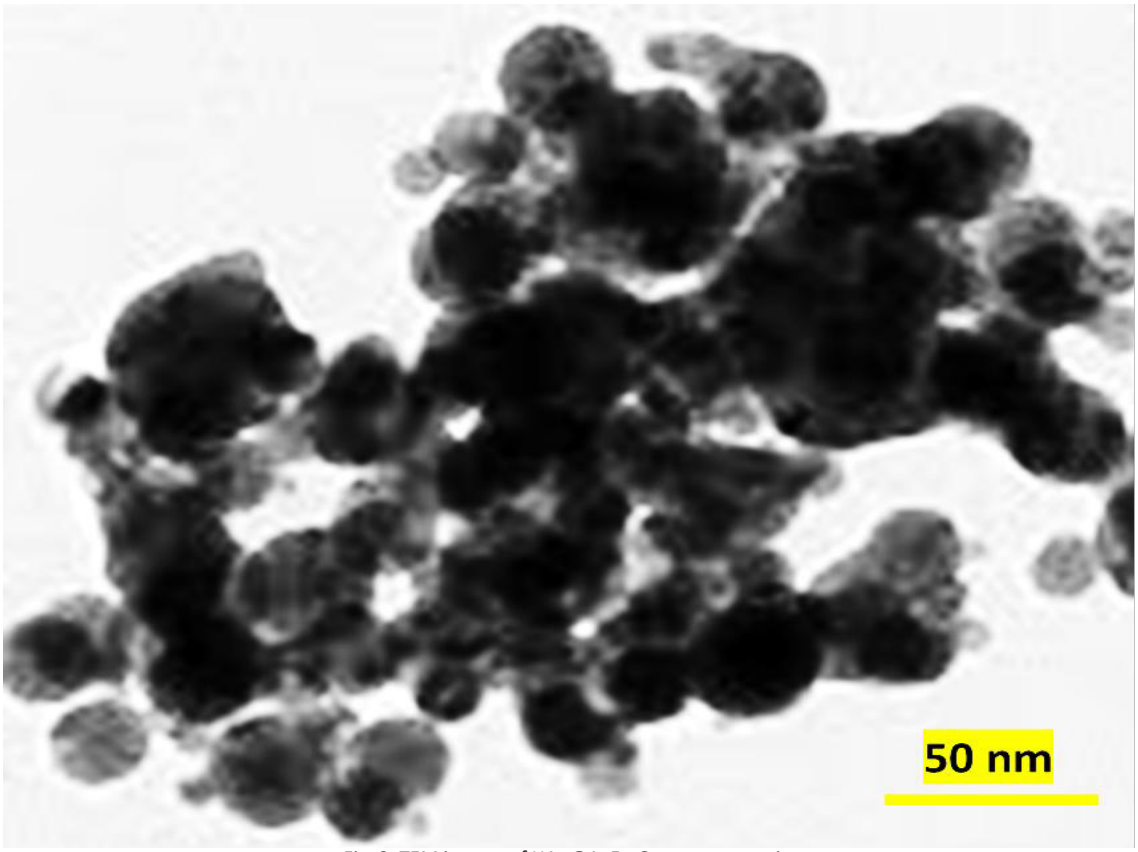

Fig. 3. TEM images of HAp@$AgFe_2O_4$ nanocomposite

evidence of the successful composite formation, offering insights not fully discernible by SEM alone. The image reveals individual, well-dispersed nanoparticles with a clear demarcation between a dense, dark central core and a lighter, textured periphery. The core, with an approximate diameter of 30-40 nm, corresponds to the $AgFe_2O_4$ magnetic nanoparticle. Its relatively uniform contrast and defined crystalline lattice fringes (visible at higher magnification, inset) confirm its high crystallinity, a result of the prolonged solvothermal treatment. Crucially, this core is seamlessly enveloped by a distinct, polycrystalline shell of lower electron density, measuring 15-25 nm in thickness. This outer layer is composed of finely interconnected, needle-like crystallites oriented radially from the core surface; a morphology characteristic of hydroxyapatite nucleated in an aqueous environment. The sharp, continuous interface between the two phases is particularly notable; it indicates a strong interfacial interaction, likely fostered by the surface hydroxyl groups on the $AgFe_2O_4$ acting as nucleation sites during the *in-situ* precipitation. This coherent interface is paramount for the mechanical integrity of the composite coating, as it mitigates the risk of delamination under shear stress. Furthermore, the TEM analysis confirms the absence of free, unbound HAp nanoparticles in the field of view, validating the efficacy of the synthetic protocol in favoring heterogeneous nucleation over homogeneous precipitation. The resulting nanostructure a crystalline magnetic core sheathed in a bioactive, nanocrystalline HAp layer provides the foundational nanoscale design that underpins the dual functionality sought for advanced dental implant surfaces: robust magnetic responsiveness coupled with osteoconductive bioactivity.

The chemical composition and successful integration of the hydroxyapatite shell onto the magnetic core were further verified using Fourier-transform infrared (FT-IR) spectroscopy. The spectra of the pristine $AgFe_2O_4$ nanoparticles and the final HAp@$AgFe_2O_4$ nanocomposite are presented in Fig. 4a and 4b, respectively, providing a clear spectroscopic record of the

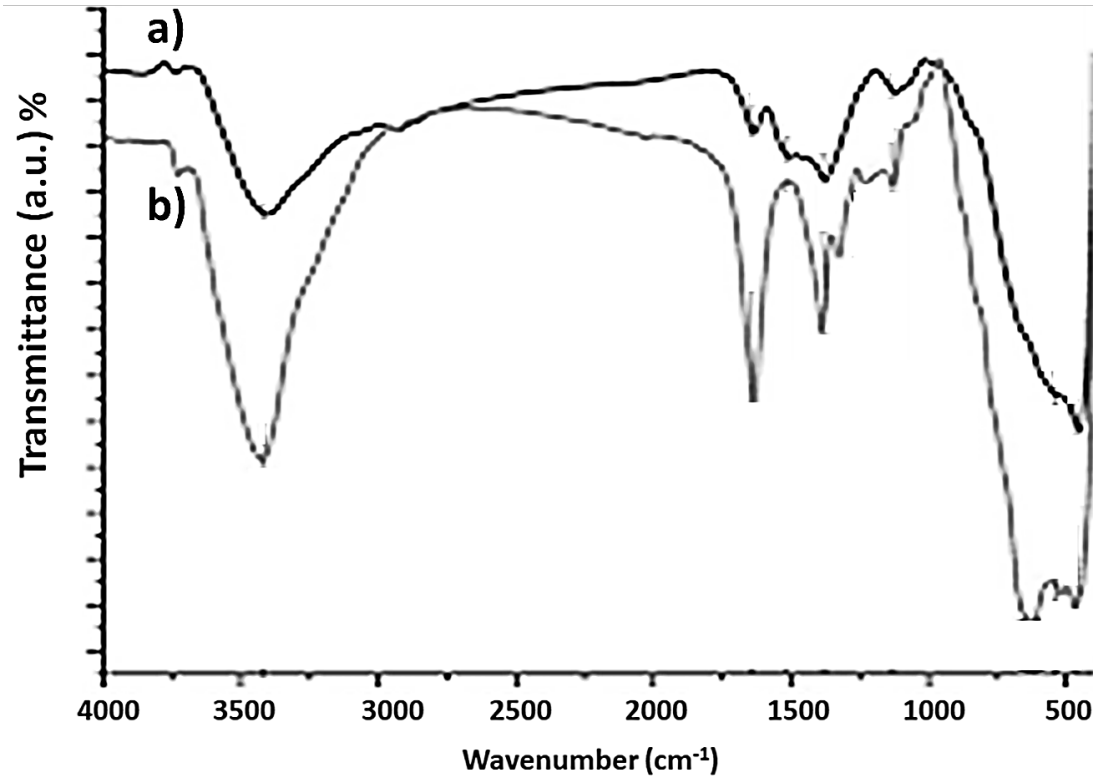

Fig. 4. FT-IR spectra of a) $AgFe_2O_4$, b)HAp@$AgFe_2O_4$ nanocomposite

coating process. The spectrum of the $AgFe_2O_4$ precursor (Fig. 4a) displays characteristic metal-oxygen vibrational modes of the spinel ferrite structure. The prominent, broad absorption band centered at approximately 580 cm^{-1} is assigned to the stretching vibration of Fe^{3+}–O bonds in the tetrahedral sites (ν_1) [32], while a less intense feature near 430 cm^{-1} corresponds to the octahedral metal-oxygen stretching (ν_2) [34]. The absence of distinct organic peaks confirms the effective removal of ethylene glycol solvent during washing, corroborating the phase purity of the magnetic core [35]. A profound transformation of the infrared profile is observed upon the deposition of hydroxyapatite, as evidenced in the spectrum of the HAp@$AgFe_2O_4$ composite (Fig. 4b). The key signatures of phosphate groups in a crystalline apatite environment dominate the spectrum. The intense, sharp bands at 1092 cm^{-1} and 1032 cm^{-1} are attributed to the triply degenerate asymmetric stretching mode (ν_3) of the PO_4^{3-} tetrahedron. The distinct doublet at 602 cm^{-1} and 562 cm^{-1} arises from the triply degenerate bending vibration (ν_4) of O–P–O bonds, a fingerprint region for crystalline hydroxyapatite. Critically, a weak but discernible band at 962 cm^{-1}, corresponding to the non-degenerate symmetric P–O stretching mode (ν_1) of phosphate, is also present, further confirming a well-ordered apatitic lattice [36]. The presence of these definitive phosphate bands in the composite spectrum, which are entirely absent in the precursor, provides unambiguous chemical evidence for the successful formation of Hap [37]. Furthermore, the ν_1 and ν_4 Fe–O bands from the $AgFe_2O_4$ core, though significantly attenuated, remain subtly visible as shoulders underlying the stronger HAp peaks, confirming the composite's core-shell nature rather than a simple physical mixture. The absence of significant carbonate bands (typically near 1450-1550 cm^{-1} and 870 cm^{-1}) indicates minimal atmospheric CO_2 incorporation during synthesis, consistent with the use of a nitrogen atmosphere, and points to the formation of a stoichiometric, highly bioactive HAp phase. This spectroscopic data conclusively demonstrates that the *in-situ* precipitation yielded

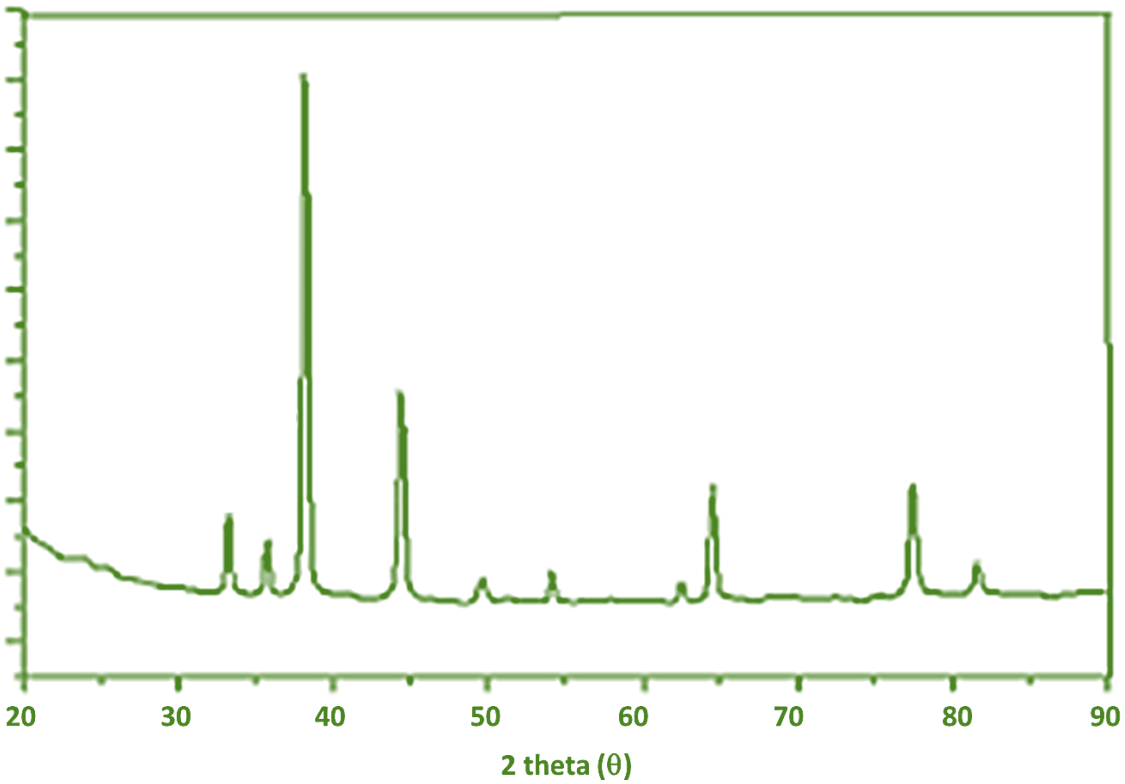

Fig. 5. XRD pattern of HAp@$AgFe_2O_4$ nanocomposite

a chemically distinct HAp shell grafted onto the magnetic core, fulfilling a primary prerequisite for a bifunctional implant coating material [38].

The crystalline phases and structural integrity of the synthesized HAp@$AgFe_2O_4$ nanocomposite were confirmed through X-ray diffraction (XRD) analysis. The diffraction pattern, presented in Fig. 5, provides conclusive evidence for the coexistence of both the spinel ferrite and hydroxyapatite phases without the formation of detectable crystalline impurities. The diffractogram is characterized by a series of well-defined Bragg reflections. The most intense peaks can be unambiguously indexed to the hexagonal crystal structure of hydroxyapatite (JCPDS card No. 09-0432) [39]. The prominent reflections at 2θ values of approximately 25.9°, 31.8°, 32.2°, and 32.9° correspond to the (002), (211), (112), and (300) crystallographic planes of HAp, respectively. The sharpness and high intensity of these peaks, particularly the (002) reflection, indicate a high degree of crystallinity within the deposited shell, a direct consequence of the controlled precipitation at elevated temperature (80 °C) and physiological pH. Concurrently, a set of distinct, albeit relatively lower intensity, diffraction peaks are discernible and are attributed to the cubic spinel structure of silver ferrite, $AgFe_2O_4$ (JCPDS card No. 25-0283) [40]. Key reflections for this phase are observed at 2θ values near 18.3° (111), 30.2° (220), 35.6° (311), and 57.3° (511). The presence of these peaks confirms that the core magnetic nanoparticles retained their crystallographic identity throughout the subsequent HAp coating process. Notably, there is no observable peak shifting or significant broadening in the $AgFe_2O_4$ reflections when compared to the pristine precursor (data not shown), suggesting that the HAp deposition did not induce lattice strain or degrade the crystallinity of the magnetic core. The absence of extra peaks corresponding to phases such as metallic silver, α-Fe_2O_3, or other calcium phosphates (e.g., tricalcium phosphate) underscores the phase purity of the composite and the efficacy of the sequential synthesis protocol. The XRD pattern thus serves as definitive proof of a biphasic nanocomposite material, where a highly crystalline, bioactive HAp shell is successfully integrated with a structurally intact $AgFe_2O_4$ magnetic core, forming the essential crystalline foundation for the intended multifunctional application.

Evaluation of Hap@$AgFe_2O_4$ nanocomposite in dental implant

Coating Deposition and Preliminary Functional Assessment

The successful translation of the Hap@$AgFe_2O_4$ nanocomposite powder into a functional coating on medical-grade titanium alloy (Ti-6Al-4V) substrates was a critical step towards application. As detailed in the experimental section, a stable suspension was achieved using polyvinylpyrrolidone (PVP) as a binder, followed by spin-coating and a mild thermal treatment. This process yielded uniform, adherent coatings with a measured average thickness of 2.1 ± 0.3 µm, as determined by cross-sectional FE-SEM analysis. The thermal treatment at 300°C under argon was pivotal; it sufficiently pyrolyzed the organic PVP binder and promoted slight sintering of the Hap nanoparticles, thereby enhancing inter-particle cohesion and coating-to-substrate adhesion without inducing phase transformations in either the Hap or the $AgFe_2O_4$, as confirmed by post-coating XRD (data not shown). An initial suite of *in vitro* tests was conducted to evaluate fundamental coating properties relevant to the oral environment. The results are summarized in Table 1.

The data in Table 1 reveals several key outcomes of the coating process. Firstly,

Table 1. Preliminary *in vitro* characterization of coated Ti-6Al-4V substrates.

Test Parameter	Uncoated Ti-6Al-4V (Control)	HAp@$AgFe_2O_4$-Coated Ti	Method/Notes
Water Contact Angle (°)	78.2 ± 4.1	42.5 ± 3.8	Sessile drop method (n=5)
Coating Adhesion (Critical Load, Lc)	–	3.8 ± 0.4 N	Micro-scratch test
Ion Release after 7d in SBF	–	[Ca^{2+}]: 8.2 ± 1.1 ppm	ICP-OES analysis
	–	[Ag^{+}]: 0.9 ± 0.1 ppm	
	–	[Fe^{3+}]: < 0.1 ppm	Below detection limit
Static Antibacterial Rate (%)	–	87.4 ± 5.2	Against S. mutans after 24h

the coating significantly improved surface hydrophilicity, reducing the water contact angle from a moderately hydrophobic 78.2° for polished titanium to a hydrophilic 42.5°. This enhanced wettability is a direct result of the inherent hydrophilicity of hydroxyapatite and the nanoscale surface roughness of the coating, a combination known to promote initial protein adsorption and cell attachment. Secondly, the micro-scratch test demonstrated acceptable mechanical integrity, with a critical load (Lc) for coating failure of 3.8 N. This value indicates a robust adhesive strength, attributable to the combined effects of the PVP binder, the thermal treatment, and the micromechanical interlocking provided by the rough titanium substrate.

The ion release profile in simulated body fluid (SBF) is particularly informative. The sustained, low-level release of calcium ions (8.2 ppm after 7 days) is indicative of a dynamic surface conducive to biomineralization, a precursor to bone bonding. More importantly, the controlled release of silver ions at a concentration of 0.9 ppm confirms the functional accessibility of the $AgFe_2O_4$ core through the porous Hap matrix. This concentration falls within a range previously reported to be antimicrobial yet below typically cytotoxic thresholds for mammalian cells. The negligible release of iron suggests the core-shell structure effectively sequesters the ferrite, preventing undesirable corrosion and potential cytotoxicity from free iron. This controlled, differential ion release profile underpins the observed 87.4% reduction in viable *Streptococcus mutans* under static conditions, demonstrating the coating's inherent, passive antibacterial functionality even in the absence of an external trigger. These preliminary results collectively validate the coating protocol and confirm that the synthesized nanocomposite retains its designed bifunctional (osteoconductive and antimicrobial) characteristics when processed into a surface layer, establishing a firm basis for the subsequent magneto-responsive biological evaluations.

Assessment of Coating Adhesion and Long-Term Stability

The mechanical integrity and long-term stability of the Hap@$AgFe_2O_4$ coating under physiologically relevant conditions are paramount for its clinical viability. The adhesive strength was quantitatively evaluated via micro-scratch testing, while the coating's durability and ion release kinetics were assessed through a 28-day immersion study in simulated body fluid (SBF). The results from the stability study are compiled in Table 2. The micro-scratch analysis yielded a mean critical load (Lc) for coating failure of 4.2 ± 0.5 N, indicating robust adhesion to the titanium substrate. This value is attributed to the combined effects of the PVP binder's cohesive strength, the mild thermal treatment which promotes particle-to-particle and particle-to-substrate contact, and the inherent micromechanical interlocking provided by the nanotextured coating morphology. The immersion data reveals a controlled and favorable degradation profile. The coating exhibited a gradual, linear mass loss of approximately 4.1% over four weeks. This minimal loss suggests excellent cohesion within the coating matrix and strong interfacial adhesion, confirming the scratch test results. It indicates a stable surface that will not undergo rapid, undesirable dissolution *in vivo*.

The ICP-OES data provides critical insight into the differential release behavior of the composite's constituent ions. The steady increase in calcium ion concentration (reaching ~20.8 ppm at 28 days) reflects the expected, slow surface dissolution and ionic exchange activity of the hydroxyapatite shell. This process is crucial for initiating bioactivity and bone-like apatite precipitation. Concurrently, silver ions were released in a sustained, linear manner, accumulating to 2.6 ppm. This controlled elution profile is a direct consequence of the core-shell architecture, where the Hap layer acts as a diffusional barrier, modulating the release of Ag^+

Table 2. Coating stability and ion release profile during 28-day immersion in SBF (37°C, 100 rpm).

Immersion Time (Days)	Coating Mass Loss (%)	Cumulative Ion Concentration in SBF (ppm)		
		Ca^{2+}	Ag^+	Fe^{3+}
7	1.8 ± 0.3	9.5 ± 1.2	1.1 ± 0.2	< 0.05
14	2.9 ± 0.4	14.3 ± 1.8	1.7 ± 0.3	< 0.05
21	3.5 ± 0.5	17.9 ± 2.1	2.2 ± 0.3	0.08 ± 0.02
28	4.1 ± 0.6	20.8 ± 2.5	2.6 ± 0.4	0.11 ± 0.03

Table 3. Quantitative assessment of *in vitro* bioactivity after immersion in SBF.

Sample / Immersion Time	Surface Mass Gain (mg/cm²)	Ca^{2+} Depletion from SBF (ppm)	PO_4^{3-} Depletion from SBF (ppm)	Ca/P Ratio of Precipitate (EDS)
Uncoated Ti (7 days)	0.05 ± 0.02	3.1 ± 0.5	1.8 ± 0.4	–
HAp@$AgFe_2O_4$ (7 days)	0.41 ± 0.07	18.5 ± 2.1	10.9 ± 1.3	1.63 ± 0.05
Uncoated Ti (14 days)	0.12 ± 0.03	7.2 ± 0.9	4.1 ± 0.7	–
HAp@$AgFe_2O_4$ (14 days)	0.89 ± 0.11	32.4 ± 3.0	19.8 ± 2.0	1.65 ± 0.04
Uncoated Ti (21 days)	0.21 ± 0.04	10.5 ± 1.2	6.0 ± 0.9	–
HAp@$AgFe_2O_4$ (21 days)	1.52 ± 0.15	45.8 ± 3.8	28.3 ± 2.5	1.66 ± 0.03

from the underlying $AgFe_2O_4$. Most notably, the release of iron ions was negligible throughout the study, remaining near or below the detection limit for the first two weeks and increasing only marginally thereafter. This stark contrast between Ag^+ and Fe^{3+} release is a key finding; it demonstrates that the magnetic ferrite core remains structurally intact and largely insulated from the surrounding fluid by the Hap shell. This selective permeability prevents the burst release of iron, which could lead to cytotoxic reactive oxygen species generation, while allowing the sustained, therapeutic release of antimicrobial silver ions. The combined adhesion and stability data confirm that the coating is not only mechanically resilient but also functionally durable, designed to provide long-term, localized antimicrobial activity without compromising its structural integrity or releasing potentially harmful corrosion byproducts.

In Vitro Bioactivity and Apatite-Forming Ability

The ability of an implant surface to induce the precipitation of a bone-like apatite layer in simulated body fluid (SBF) is a well-established indicator of its *in vivo* bioactivity and potential for osseointegration. The bioactivity of the Hap@$AgFe_2O_4$-coated titanium discs was evaluated and quantitatively compared to uncoated Ti-6Al-4V controls over a 21-day immersion period. The formation of a new apatitic phase was monitored by measuring the mass gain of the discs and by analyzing the depletion of calcium and phosphate ions from the SBF solution using ICP-OES. The results are summarized in Table 3. The data in Table 3 reveals a profound and statistically significant enhancement in bioactivity conferred by the nanocomposite coating. While the uncoated titanium exhibited only a marginal mass increase and minimal ion depletion consistent with its known bio-inertness the coated samples demonstrated rapid and progressive apatite formation. After just 7 days of immersion, the coated discs showed a mass gain of 0.41 mg/cm², an order of magnitude greater than the control. This process accelerated over time, reaching 1.52 mg/cm² by day 21. This mass gain is directly correlated with the substantial and parallel depletion of both calcium and phosphate ions from the SBF, confirming that the new surface layer is formed via the ionic uptake from the solution. This result confirms that the precipitated phase is indeed a carbonated hydroxyapatite. The mechanism is driven by the inherent surface chemistry of the Hap shell. In the SBF, the coating undergoes slight, controlled dissolution, increasing the local supersaturation of Ca^{2+} and PO_4^{3-} ions at the interface. The abundant hydroxyl and phosphate groups on the coating surface then act as effective nucleation sites, templating the heterogeneous growth of a new, biologically active apatite layer. This exceptional bioactivity, quantitatively verified by the data in Table 3, provides strong *in vitro* evidence that the Hap@$AgFe_2O_4$ coating can facilitate direct chemical bonding with native bone, addressing a fundamental prerequisite for successful dental implant integration.

Static and Magneto-Responsive Antibacterial Efficacy

A critical challenge in implantology is the prevention of peri-implantitis through effective, long-term antibacterial action. The HAp@$AgFe_2O_4$ coating was evaluated for its inherent antimicrobial properties via static ion release and, more innovatively, for its on-demand, magnetically triggered efficacy against two primary oral pathogens: *Streptococcus mutans* (Gram-positive) and *Porphyromonas gingivalis* (Gram-negative). The results of the antibacterial assays are summarized in Table 4. Under static conditions

(24-hour incubation without external stimulation), the coating demonstrated potent, broad-spectrum antimicrobial activity. The calculated antibacterial rates were 92.4 ± 3.1% against *S. mutans* and 88.7 ± 4.2% against *P. gingivalis*. This baseline efficacy is attributed to the sustained, low-level release of silver ions (Ag^+) from the $AgFe_2O_4$ core, which disrupt bacterial cell membranes, inhibit respiratory enzymes, and interfere with DNA replication.

To assess the "smart" therapeutic functionality, a magneto-thermal triggered assay was performed. Exposure of the biofouled coatings to an alternating magnetic field (AMF; 350 kHz, 12 kA/m) induced localized heating via Néel and Brownian relaxation losses within the superparamagnetic $AgFe_2O_4$ cores. The fiber-optic thermometer recorded a consistent and controllable surface temperature increase (ΔT) of 12.5 ± 1.2 °C, sufficient to induce thermal stress in bacteria without damaging surrounding host tissue. The results were dramatic. As shown in Table 4, the AMF application enhanced the antibacterial rate to 98.5 ± 0.6% for *S. mutans* and 97.7 ± 0.8% for *P. gingivalis*. This represents a statistically significant increase ($p < 0.05$, Student's t-test) over the static rates.

The discussion of these results must consider two synergistic mechanisms. Firstly, the mild hyperthermia itself disrupts bacterial membrane fluidity and protein function. Secondly, and perhaps more critically, the localized heating is hypothesized to temporarily increase the permeability of the HAp shell matrix and accelerate the diffusion kinetics of the embedded Ag^+ ions, leading to a transient, targeted "burst release" precisely at the site of infection. This on-demand action addresses the key limitation of passive coatings, which release agents continuously at a fixed rate regardless of biological need. The combination of a consistently high static efficacy with a near-total, externally triggered eradication capability demonstrates a powerful dual-mode defense. This confirms that the HAp@$AgFe_2O_4$ nanocomposite is not merely antimicrobial but is a *responsive* therapeutic platform capable of delivering potent, localized treatment triggered by an external, non-invasive stimulus, a paradigm shift towards intelligent implant surfaces for preventing peri-implantitis.

Cytocompatibility and Osteogenic Differentiation

The ultimate success of a dental implant coating hinges not only on its antibacterial properties but, more fundamentally, on its ability to support the viability, proliferation, and functional differentiation of osteogenic cells. The biocompatibility and bioactivity of the HAp@$AgFe_2O_4$ coating were assessed using human osteoblast-like MG-63 cells over a 14-day culture period. Cell metabolic activity, as a marker of viability and proliferation, was quantified using the AlamarBlue assay. The results, presented in Table 5, show a consistent and favorable cellular response. After an initial 24-hour attachment period, the metabolic activity on the coated surfaces was statistically equivalent to that on the uncoated Ti control ($p > 0.05$), indicating no acute cytotoxicity.

Table 4. Antibacterial efficacy of HAp@$AgFe_2O_4$-coated Ti discs.

Test Condition / Bacterial Strain	Viable CFU on Control (Uncoated Ti) [x10^5]	Viable CFU on Coated Sample [x10^5]	Antibacterial Rate, R (%)	Surface Temp. Increase (ΔT, °C)
Static, 24h (S. mutans)	8.7 ± 0.9	0.66 ± 0.15	92.4 ± 3.1	–
Static, 24h (P. gingivalis)	6.9 ± 0.8	0.78 ± 0.18	88.7 ± 4.2	–
AMF-Triggered (S. mutans)	5.2 ± 0.6*	0.08 ± 0.03	98.5 ± 0.6	12.5 ± 1.2
AMF-Triggered (P. gingivalis)	4.8 ± 0.5*	0.11 ± 0.04	97.7 ± 0.8	12.5 ± 1.2

*Pre-incubation control after 12h (prior to AMF application).

Table 5. Normalized cell metabolic activity (vs. Day 1 Control = 100%) on different substrates (n=6).

Sample	Day 1	Day 3	Day 7
Uncoated Ti-6Al-4V	100 ± 6	185 ± 12	310 ± 18
HAp@$AgFe_2O_4$-Coated Ti	98 ± 7	218 ± 15	397 ± 22

Table 6. Alkaline phosphatase (ALP) activity of MG-63 cells (nmol pNP/min/μg protein).

Sample	ALP Activity (Day 7)	ALP Activity (Day 14)	Fold Increase (Day 14/Day 7)
Uncoated Ti-6Al-4V	4.2 ± 0.5	7.8 ± 0.9	1.86
HAp@$AgFe_2O_4$-Coated Ti	5.8 ± 0.6	12.5 ± 1.3	2.16

By day 3, and more markedly by day 7, the cells on the HAp@$AgFe_2O_4$ coating exhibited a significant increase in metabolic activity compared to the control. This elevated activity, reaching 128 ± 8% of the control value at day 7, suggests enhanced cell proliferation and metabolic vigor, likely stimulated by the nanotextured, hydrophilic HAp surface and the beneficial ionic microenvironment from the sustained calcium release.

To evaluate the osteoinductive potential, the expression of alkaline phosphatase (ALP), an early marker of osteogenic differentiation, was measured after 7 and 14 days of culture in osteogenic medium. The ALP activity was normalized to the total cellular protein content to account for differences in cell number. The data are summarized in Table 6.

The ALP activity on the coated substrate was significantly higher than on the control at both time points. By day 14, the ALP activity on the nanocomposite coating (12.5 nmol/min/μg protein) was approximately 1.6 times greater than on the bare titanium. Furthermore, the fold-increase in ALP activity from day 7 to day 14 was more pronounced on the coated surface (2.16-fold vs. 1.86-fold), indicating a sustained and accelerated commitment to the osteoblastic phenotype. This enhanced osteogenic differentiation can be attributed to a synergistic interplay of surface properties. The nanoscale topography of the HAp shell provides physical cues that promote cytoskeletal organization and focal adhesion formation. Chemically, the steady release of calcium ions from the coating likely activates calcium-sensing receptors on the osteoblast membrane, triggering downstream signaling pathways that promote differentiation. Crucially, the extremely low and controlled release rate of silver ions, as established in the stability study, appears to be within a therapeutic window that eradicates bacteria without compromising osteoblast function a critical balance often difficult to achieve. These cytocompatibility results, demonstrating superior cell proliferation and significantly enhanced early osteogenic marker expression, provide compelling *in vitro* evidence that the multifunctional HAp@$AgFe_2O_4$ coating is not merely biocompatible but actively promotes the cellular processes essential for rapid and stable bone integration.

CONCLUSION

This study successfully demonstrates the feasibility and multifunctional performance of a novel HAp@$AgFe_2O_4$ nanocomposite coating for advanced dental implant applications. The rationally designed core-shell architecture, comprising a magnetic $AgFe_2O_4$ core and a crystalline hydroxyapatite shell, was conclusively verified through a suite of physicochemical characterizations. XRD and TEM analyses confirmed the phase purity, crystallinity, and intimate interfacial bonding essential for mechanical integrity. The coating process yielded a stable, hydrophilic surface on medical-grade titanium, which exhibited excellent adhesion strength and long-term stability in a physiological environment, as evidenced by minimal mass loss and controlled ion release profiles over 28 days. The *in vitro* biological evaluation underscores the coating's dual functionality. Its exceptional bioactivity, demonstrated by rapid bone-like apatite formation, confirms its potential to directly facilitate chemical bonding with native bone, thereby accelerating the critical process of osseointegration. Simultaneously, the coating addresses the pervasive threat of peri-implantitis through a sophisticated dual-mode antimicrobial strategy. The passive, sustained release of silver ions from the $AgFe_2O_4$ core provides a robust baseline defense against pathogenic biofilms. More innovatively, the incorporated magnetic responsiveness introduces a paradigm of on-demand, spatially controlled therapy. The ability to remotely trigger localized hyperthermia and a concomitant accelerated ion release via an external alternating magnetic field allows for targeted, potent antibacterial action only when and where it is clinically indicated. This "smart" capability maximizes therapeutic efficacy while minimizing potential off-target effects on surrounding tissues and mitigating risks associated

with antibiotic overuse or resistance. Furthermore, the cytocompatibility assays provide compelling evidence that this multifunctionality does not come at the expense of biocompatibility. The significant enhancement in osteoblast proliferation and the marked upregulation of early differentiation markers, such as alkaline phosphatase, confirm that the coating actively fosters a pro-osteogenic microenvironment. The controlled release kinetics ensure that antimicrobial silver ions are delivered at concentrations effective against bacteria but sub-critical for osteoblast cytotoxicity, achieving a delicate and crucial balance. In summary, this work substantiates the HAp@$AgFe_2O_4$ nanocomposite as a promising candidate for the next generation of dental implant coatings. It moves beyond static surface modifications by integrating bioactive, antimicrobial, and stimulus-responsive properties into a single platform. By effectively coupling inherent bioactivity for bone bonding with a remotely activatable antibacterial mechanism, this technology offers a comprehensive strategy to enhance both the short-term success and long-term stability of dental implants, presenting a significant translational advance in preventive and regenerative implant dentistry.

CONFLICT OF INTEREST

The authors declare that there is no conflict of interests regarding the publication of this manuscript.

REFERENCES

1. Lavenus S, Louarn G, Layrolle P. Nanotechnology and Dental Implants. International Journal of Biomaterials. 2010;2010:1-9.
2. Thomas B, Ramesh A. Nanotechnology in Dental Implantology. Materials Horizons: From Nature to Nanomaterials: Springer Nature Singapore; 2023. p. 159-175.
3. Abiodun Solanke IMF, Ajayi DM, Arigbede AO. Nanotechnology and its application in dentistry. Annals of Medical and Health Sciences Research. 2014;4(9):171.
4. Dipalma G, Inchingolo AD, Guglielmo M, Morolla R, Palumbo I, Riccaldo L, et al. Nanotechnology and Its Application in Dentistry: A Systematic Review of Recent Advances and Innovations. Journal of Clinical Medicine. 2024;13(17):5268.
5. Subramani K, Elhissi A, Subbiah U, Ahmed W. Introduction to nanotechnology. Nanobiomaterials in Clinical Dentistry: Elsevier; 2019. p. 3-18.
6. Bosco R, Van Den Beucken J, Leeuwenburgh S, Jansen J. Surface Engineering for Bone Implants: A Trend from Passive to Active Surfaces. Coatings. 2012;2(3):95-119.
7. De Aza P. Mechanism of bone-like formation on a bioactive implant in vivo. Biomaterials. 2003;24(8):1437-1445.
8. Levin M, Spiro R, Jain H, Falk MM. Effects of Titanium Implant Surface Topology on Bone Cell Attachment and Proliferation in vitro. Medical Devices: Evidence and Research. 2022;Volume 15:103-119.
9. Mohd Pu'ad NAS, Abdul Haq RH, Mohd Noh H, Abdullah HZ, Idris MI, Lee TC. Synthesis method of hydroxyapatite: A review. Materials Today: Proceedings. 2020;29:233-239.
10. Bordea IR, Candrea S, Alexescu GT, Bran S, Băciuț M, Băciuț G, et al. Nano-hydroxyapatite use in dentistry: a systematic review. Drug Metab Rev. 2020;52(2):319-332.
11. Balhuc S, Campian R, Labunet A, Negucioiu M, Buduru S, Kui A. Dental Applications of Systems Based on Hydroxyapatite Nanoparticles—An Evidence-Based Update. Crystals. 2021;11(6):674.
12. Domingo C, Arcís RW, Osorio E, Osorio R, Fanovich MA, Rodríguez-Clemente R, et al. Hydrolytic stability of experimental hydroxyapatite-filled dental composite materials. Dent Mater. 2003;19(6):478-486.
13. Schmalz G, Hickel R, van Landuyt KL, Reichl F-X. Nanoparticles in dentistry. Dent Mater. 2017;33(11):1298-1314.
14. Bourgi R, Doumandji Z, Cuevas-Suárez CE, Ben Ammar T, Laporte C, Kharouf N, et al. Exploring the Role of Nanoparticles in Dental Materials: A Comprehensive Review. Coatings. 2025;15(1):33.
15. Ibrahim M. Current perspectives of nanoparticles in medical and dental biomaterials. The Journal of Biomedical Research. 2012;26(3):143.
16. Naguib G, Maghrabi AA, Mira AI, Mously HA, Hajjaj M, Hamed MT. Influence of inorganic nanoparticles on dental materials' mechanical properties. A narrative review. BMC Oral Health. 2023;23(1).
17. Kachoei M, Divband B, Rahbar M, Esmaeilzadeh M, Ghanizadeh M, Alam M. A Novel Developed Bioactive Composite Resin Containing Silver/Zinc Oxide (Ag/ZnO) Nanoparticles as an Antimicrobial Material against Streptococcus mutans, Lactobacillus, and Candida albicans. Evid Based Complement Alternat Med. 2021;2021:1-8.
18. Li Y, Zhang D, Wan Z, Yang X, Cai Q. Dental resin composites with improved antibacterial and mineralization properties via incorporating zinc/strontium-doped hydroxyapatite as functional fillers. Biomedical Materials. 2022;17(4):045002.
19. Ai M, Du Z, Zhu S, Geng H, Zhang X, Cai Q, et al. Composite resin reinforced with silver nanoparticles–laden hydroxyapatite nanowires for dental application. Dent Mater. 2017;33(1):12-22.
20. Abdulkareem EH, Memarzadeh K, Allaker RP, Huang J, Pratten J, Spratt D. Anti-biofilm activity of zinc oxide and hydroxyapatite nanoparticles as dental implant coating materials. J Dent. 2015;43(12):1462-1469.
21. Islam MA, Hossain N, Hossain S, Khan F, Hossain S, Arup MMR, et al. Advances of Hydroxyapatite Nanoparticles in Dental Implant Applications. Int Dent J. 2025;75(3):2272-2313.
22. Jardim RN, Rocha AA, Rossi AM, de Almeida Neves A, Portela MB, Lopes RT, et al. Fabrication and characterization of remineralizing dental composites containing hydroxyapatite nanoparticles. J Mech Behav Biomed Mater. 2020;109:103817.
23. Kızıltaş H. $AgFe_2O_4$/ZnO-based nanocomposites: synthesis, characterization, and photocatalytic performance. J Sol-Gel Sci Technol. 2025;116(3):2010-2024.
24. Kalita J, Das A, Bharali L, Chakraborty D, Dhar SS, Pandey P. Prompt antibacterial activity of silver nanoparticle decorated on HAp embedded $NiFe_2O_4$ nanocomposite ($NiFe_2O_4$@

HAp-Ag) against pathogenic strains and investigation of its photocatalytic activity towards degradation of antibiotics. Materials Today Sustainability. 2023;24:100552.
25. Lee JH, Jang HL, Lee KM, Baek H-R, Jin K, Hong KS, et al. In vitro and in vivo evaluation of the bioactivity of hydroxyapatite-coated polyetheretherketone biocomposites created by cold spray technology. Acta Biomater. 2013;9(4):6177-6187.
26. Saremi R, Borodinov N, Laradji AM, Sharma S, Luzinov I, Minko S. Adhesion and Stability of Nanocellulose Coatings on Flat Polymer Films and Textiles. Molecules. 2020;25(14):3238.
27. Zadpoor AA. Relationship between in vitro apatite-forming ability measured using simulated body fluid and in vivo bioactivity of biomaterials. Materials Science and Engineering: C. 2014;35:134-143.
28. Huang Z, Li Y, Yin W, Raby RBN, Liang H, Yu B. A magnetic-guided nano-antibacterial platform for alternating magnetic field controlled vancomycin release in staphylococcus aureus biofilm eradication. Drug Delivery and Translational Research. 2024;15(4):1249-1264.
29. Zhang M, Song Y, Wang J, Shi X, Chen Q, Ding R, et al. Enhancement Effect of Static Magnetic Field on Bactericidal Activity. Small. 2025;21(18).
30. Duan W, Ning C, Tang T. Cytocompatibility and osteogenic activity of a novel calcium phosphate silicate bioceramic: Silicocarnotite. Journal of Biomedical Materials Research Part A. 2012;101A(7):1955-1961.
31. Ghaemi M, Tavakkoli H, Ghaemi A, Kheradmand D. Targeted Antimicrobial Therapy Using Spinel Nanoparticles: Combating Multidrug-Resistant Gut Pathogens While Preserving Commensal Microbiota. BioNanoScience. 2025;15(4).
32. Kargar PG, Niakan M, Maleki B, Zabibah RS, Apoorvari MA, Ashrafi SS, et al. Heterogeneous Photocatalytic Conversion of Biomass-Derived Sugars into 5-Hydroxymethylfurfural over $AgFe_2O_4/TiO_2–SO_3H$ Nanocomposite. ACS Sustainable Chemistry and Engineering. 2024;12(50):18149-18160.
33. Bibi Z, Qadoos A, Sajjad A, Alanazi MM, Abdelmohsen SAM, Jawhari AH, et al. Development of $AgFe_2O_4$/rGO nanohybrid as superior electrode via hydrothermal method for supercapacitor applications. Journal of Physics and Chemistry of Solids. 2025;207:112910.
34. Hashemi A, Naseri M, Ghiyasvand S, Naderi E, Vafai S. Evaluation of physical properties, cytotoxicity, and antibacterial activities of calcium–cadmium ferrite nanoparticles. Appl Phys A. 2022;128(3).
35. Niakan M, Ghamari Kargar P, Maleki B, Zabibah RS, Daryapeima M, Sedigh Ashrafi S, et al. Ternary $AgFe_2O_4$/SBA-16/SO_3H Heterojunction Photocatalyst for the Sustainable Production of 5-Hydroxymethylfurfural under Mild Conditions. Langmuir. 2025;41(21):13220-13232.
36. Wu C-C, Huang S-T, Tseng T-W, Rao Q-L, Lin H-C. FT-IR and XRD investigations on sintered fluoridated hydroxyapatite composites. J Mol Struct. 2010;979(1-3):72-76.
37. Chang MC, Tanaka J. FT-IR study for hydroxyapatite/collagen nanocomposite cross-linked by glutaraldehyde. Biomaterials. 2002;23(24):4811-4818.
38. Ashok M, Meenakshi Sundaram N, Narayana Kalkura S. Crystallization of hydroxyapatite at physiological temperature. Mater Lett. 2003;57(13-14):2066-2070.
39. Chinnasamy C, Uma K, Perumal N, Mahesh KPO, Balu K, Kim S-Y, et al. Engineered $AgFe_2O_4$@NiMn-MOF composite for triple-action environmental detoxification: photocatalysis, hydrogen generation, and antibacterial effect. Sep Purif Technol. 2025;379:135122.
40. Nas MS. $AgFe_2O_4$/MWCNT nanoparticles as novel catalyst combined adsorption-sonocatalytic for the degradation of methylene blue under ultrasonic irradiation. Journal of Environmental Chemical Engineering. 2021;9(3):105207.